



Clean application of magnetic biomaterial for the removal of As (III) from water

Agnes Pholosi¹ · Bobby E. Naidoo¹ · Augustine E. Ofomaja¹

Received: 4 June 2018 / Accepted: 15 August 2018 / Published online: 29 August 2018
© Springer-Verlag GmbH Germany, part of Springer Nature 2018

Abstract

Magnetite-coated pine cone biomass was successfully synthesized, characterized, and its interaction with As (III) in water evaluated in order to apply it as an efficient adsorbent. Transmission electron microscope, scanning electron microscope, and imaging studies revealed that spherical magnetite particles were evenly distributed over the pine cone surface. Adsorption studies showed that the optimum pH of As (III) adsorption was 8 and that Fe (III) leaching was negligible at this pH. The optimum Fe₃O₄:pine cone ratio for As (III) removal was 2.0 g Fe₃O₄:1.5 g pine cone with adsorption capacity of 13.86 mg/g. The pseudo-second-order model best fitted the kinetic data with activation energy of adsorption was calculated to be 23.78 kJ/mol. The Langmuir isotherm described the equilibrium data best while the values of Dubinin–Radushkevich mean free energy suggests anion-exchange process. Increasing ionic strength slightly increased As (III) capacity of MNP-PCP from 13.86 to 17.82 mg/g at optimum solution pH of 8, but As (III) adsorption reduced by PO₄³⁻ anions and humic acid due to competition. Adsorption mechanism was confirmed with evidence from FTIR, XPS, pH_{PZC}, and NO₃⁻ replacement by As (III) adsorption onto the NO₃⁻-loaded composite.

Keywords Arsenic (III) · Anion-adsorbate interaction · Adsorption mechanism · Mean free energy · Magnetic adsorbent · Anion-exchange coefficient

Introduction

The application of arsenic (As) in agriculture has led to undesirable impact on the health of human beings and animals. Currently about 92% of the world's arsenic production is used for agricultural purposes such as herbicides and pesticides and in timber treatment (Ranjan et al. 2009). Water and wastewaters from these activities usually find their way into rivers, streams, and underground waters causing pollution. In the aqueous environment, As exists in the organic form as dimethylarsenic acid, methylarsenic acid, and arsine (Van

Vinh et al. 2015), while in the inorganic forms As exists as As (V) (arsenates), H₃AsO₃, H₃AsO₃²⁻ (arsenious), and As (III) (arsenites) (Amin et al. 2006). Generally, it is accepted that inorganic species of As are more toxic to humans than the organic forms, since most organic As pollutants can be eliminated from the body (Chung et al. 2014). The toxicity of As (III) is estimated to be 25–60 times greater than As (V) because of its affinity for sulphhydryl functional groups on enzyme systems which then blocks the actions and reactions of the groups (Ansone et al. 2013).

As (III) is usually adsorbed from aqueous solution at pH values between 6 and 8 (Ranjan et al. 2009; Zhou et al. 2014). At these pH values, the predominant As (III) specie is H₃AsO₃ which is neutral, therefore As (III) adsorption can be said not to occur by electrostatic interaction and is not easily removed as compared with As (V). Several As (III) removal methods have therefore focused attention on oxidation of As (III) to As (V) prior to adsorption and this has been associated with added complexities (Goswami et al. 2012). In recent times, studies have been focused on the use metal-loaded anion exchangers having acidic or basic functionalities (Hua et al. 2017; Peter et al. 2017). Although these have been proven effective, but there remains the challenge of the high cost of the resin.

Responsible editor: Tito Roberto Cadaval Jr

Electronic supplementary material The online version of this article (<https://doi.org/10.1007/s11356-018-2990-2>) contains supplementary material, which is available to authorized users.

✉ Augustine E. Ofomaja
aus_ofomaja@yahoo.com; augustineo@vut.ac.za

¹ Biosorption and Wastewater Treatment Research Laboratory, Department of Chemistry, Faculty of Applied and Computer Sciences, Vaal University of Technology, P. Bag X021, Vanderbijlpark 1900, South Africa

Biomaterials have therefore been introduced as cheap, readily available, and eco-friendly alternative support for the more expensive anion-exchange resins. Biomaterials such as agricultural wastes materials carry functional groups (acidic or basic) on their surfaces which makes them capable to supporting metal oxides and hydroxides such as iron oxide on coconut (*Cocos nucifera* L.) fiber (Nashine and Tembhurkar 2016), Lanthanum oxide on sawdust (Setyono and Valiyaveetil 2014), and Zr (VI) oxide on orange waste gel (Biswas et al. 2008) have been applied. Although studies suggests that effective removal of As (III) with supported metal oxides depends on the type of metal oxide (Biswas et al. 2008; Yoshida 1981), Kumar et al. (2014) showed that the ability of metal oxide interaction with As (III) was not dependent on the number of hydroxyl functional groups on the metal oxide or its surface area, but on the metal oxides ionic potential (charge of ion divided by its radius, Å). Fang et al. (2003) reported that the support materials for metal oxides applied in the removal of oxyanion adsorption greatly influences the adsorption process. The authors suggested that support matrixes prepared from biomass having high organic acid content showed exception affinity toward oxyanions.

This study is therefore aimed at examining the type and mechanism involved when As (III) interacts with Fe₃O₄ immobilized on pine cone biomass. As (III) adsorption was carried out using Fe₃O₄-pine cone composite having different pine cone to Fe₃O₄ ratio, temperature effect on adsorption kinetics and thermodynamic parameters were also determined. Ionic strength and anion competition at various solution pH was examined to evaluate application of Fe₃O₄-pine cone composite in the environment. Based on the experimental results, evidence of anion ligand exchange was examined using FTIR, XPS, pH_{PZC}, and trends of actual displacement of NO₃⁻ with As (III) from the NO₃⁻-loaded adsorbent.

Materials and methods

Materials

Cones from Pine tree obtained from a plantation in Vanderbijlpark South Africa were collected. The cones were de-scaled, ground in a blender, and sieved to size below 90 μm which was then used for analysis. As (III) stock solution was prepared by dissolving a weighed amount of NaAsO₂ in deionized water.

Methods

MNP-PCP

PCP was prepared by soaking a weighed amount of pine in 0.5 L of 0.15 M NaOH solution (Ofomaja et al. 2009). MNP-

PCP was prepared by adding FeSO₄·7H₂O (2.1 g) and FeCl₃·6H₂O (3.1 g) to 0.08 L of double -distilled water in a three-necked flask under inert atmosphere with continuous stirring at 200 rpm. The mixture was then heated to 60 °C after which 0.03 L of 25% ammonium hydroxide and 1.5 g PCP were added. The heating and stirring at 60 °C was continued for further 30 min. The product of the reaction was then washed several times with deionized water and ethanol, then dried in a vacuum oven at 50 °C for 24 h.

Adsorbent characterization

The surface functional groups on MNP-PCP were determined using a Perkin-Elmer (USA) ATR-FTIR Spectra 400 spectrometer in the range 450–4000 cm⁻¹. Surface morphology and elemental composition was analyzed using a field emission-scanning electron microscope (FE-SEM) Carl-Zeiss-Sigma instrument (Germany). Transmission electron microscopy (TEM) image was obtained using a JEOL 2010 FET TEM (Japan). Vibrating sample magnetometer magnetic properties of MNP-PCP nanocomposite was determined with a Quantum Design MPMS-7. X-ray photoelectron spectroscopy (XPS) analysis was performed on PHI 5000 scanning ESCA microprobe with Al Kα x-ray beam (hν = 1486.6 eV). X-ray diffraction (XRD) micrograph for MNP-PCP was obtained on a Shimadzu X-ray diffractometer with CuKα anode (λ = 0.154 nm). The specific surface area of the biosorbent was measured by BET analyzer. Specific surface area of MNP-PCP was determined using a Quantachrome NovaWin (Quantachrome Instruments) surface area analyzer. Salt addition method was applied in determining the point zero charge (pH_{PZC}) of MNP-PCP.

Effect of solution pH on As (III) adsorption

Solution pH effect on As (III) removal from aqueous solution was investigated using batch adsorption study in which 0.1 L of 100 mg/L of As (III) with the initial solution pH varied between 1.0 and 10.0 using 0.1 mol/L of either HCl or NaOH solution. Accurately weighed mass of MNP-PCP (0.5 g) was agitated for 2 h in each beaker at room temperature; the mixture was then magnetically separated. Concentration of As (III) left in solution was then determined by inductively coupled plasma-optical emission spectrometry (ICP-OES). Then, 0.05 L aliquots were sampled from the suspension and passed through an arsenic speciation cartridge (Metalsoft Center, Highland Park, NJ) packed with a 2.5 g highly selective absorbent (Meng et al. 2001). The cartridge removed all As (V) but allowed As (III) to pass through in the pH range 4 to 9. Then, As (III) in the filtered solution was also determined using ICP-OES.

The influence of MNP to PCP ratio on As (III) adsorption

Effect of MNP to PCP ratio was determined by co-precipitating 2.1 g of $\text{FeSO}_4 \cdot 7\text{H}_2\text{O}$ and 3.1 g of $\text{FeCl}_3 \cdot 6\text{H}_2\text{O}$ on different masses of PCP (1.0, 1.5, 2.0, 2.5, and 3.0 g). The prepared adsorbents were applied for the adsorption of As (III) from a 100 mg/L As (III) solution at pH 8 and stirred at 200 rpm. The adsorbents were magnetically separated. As (III) remaining in the filtrate was then analyzed as above.

As (III) adsorption kinetics

Batch contact kinetic experiments were performed at reaction temperatures ranging from 26, 31, 36, 41, and 46 °C by contacting 0.5 g of the adsorbent materials with 0.1 L of As (III) solution of concentration 150 mg/L in a conical flask agitated 200 rpm for 2 h and set to pH 8.0. Aliquot (0.0001 L) of sample was withdrawn at given interval, filtered, and diluted appropriately and the As (III) analyzed as above.

Equilibrium studies of As (III) adsorption

A volume of 0.1 L of different As (III) concentrations (25 to 150 mg/L) were set at pH 8 in 0.25 L conical flasks. A mass of 0.5 g of MNP-PCP were then added separately to the solutions. The different flasks were then agitated at constant speed of 200 rpm in a shaker at different temperatures from 299, 304, 309, 313, and 319 K. At the end of 2-h agitation, the adsorbents were magnetically separated. As (III) remaining in the filtrate was then analyzed as above.

Ionic strength and competing anions

The influence of ionic strength and competing ions on As (III) adsorption onto MNP-PCP was examined by contacting 0.5 g of the adsorbents with 0.1 L of 100 mg/L As (III) solution containing 0.01, 0.05, 0.10, 0.15, and 0.20 mol/L of NaNO_3 . For the effect of anion competition, the adsorbents were contacted with 0.1 L of 0.1 mol/L of NaCl , Na_2SO_4 , Na_2CO_3 , NaNO_3 , and NaHPO_4 set at pH 8, 299 K, and shaken for 2 h.

As (III)/ NO_3^- exchange on NO_3^- -loaded MNP-PCP.

MNP-PCP (5.0 g) was dispersed in 100 mg/L NaNO_3 solution which was then stirred at 200 rpm for 5 h at pH 5 at 299 K. On completion of 5 h of stirring, the solid was washed to remove excess NaNO_3 and dried overnight at 90 °C. A mass of 0.5 g of the NO_3^- -loaded adsorbent was added to 0.1 L solutions of 0, 5, 25, 50, and 100 mol/L As (III) solutions (pH 8) and was stirred at 200 rpm at 299 K. The amounts of NO_3^- ions released in solution

and As (III) remaining were determined using an Ion selective electrode and ICP-OES.

Desorption studies

Desorption studies were carried out using residues of MNP-PCP in contact with 0.1 L of 100 mg/L of As (III) solution which was then separated by centrifugation and washed with distilled water, dried overnight, and stirred in 0.1 L of 0.5 M of each of the desorbing solvents (HCl , NaOH) and H_2O . After shaking the flask for 2 h at 200 rpm, adsorbent solids were separated by magnetic field and the leached amount of As (III) was analyzed. The amount of As (III) remaining was determined by ICP-OES.

Results and discussion

Adsorbent characterization

Transmission electron microscopy

MNP-PCP size distribution and transmission electron microscopy (TEM) images are shown in Fig. 1 while calculated size of the particles is shown in the histogram. The TEM image of MNP-PCP revealed that the magnetite nanoparticles covered the surface of the pine cone particles. The MNP particles were spherical in shape and the particles appear to be aggregated to some extent. The result shows that the mean diameter of the particles was about 7.94 nm.

Surface area (BET) analysis

The BET surface areas for the PCP and MNP-PCP were calculated as 2.25 and 54.8 m^2/g as shown in Table 1. The magnetization of the PCP caused a drastic increase in surface area and pore volume of the PCP. Such increase in BET surface area for magnetized lignocellulosic waste has been reported for orange peel powder (47.03 m^2/g) and magnetite-orange peel powder (65.19 m^2/g) (Gupta and Nayak 2012a).

Fe-SEM-EDX

Figure 2a shows the Fe-SEM images of MNP-PCP at $\times 136,000$ magnification. Figure 2a shows that MNP-PCP consisted of thick uniform layer of spherical particles covering the entire surface of the PCP particles. The micrograph indicates that the iron oxide was successfully immobilized on the PCP particles on the addition of ammonium hydroxide solution to the iron salt solution. The EDX analysis of MNP-PCP particles shown in Fig. 2b indicates the presence of carbon (C), iron (Fe), and oxygen (O), in its composition.

The dispersion of Fe on MNP-PCP is shown in the imaging in Fig. 2c. The picture in Fig. 2c shows the distribution of Fe

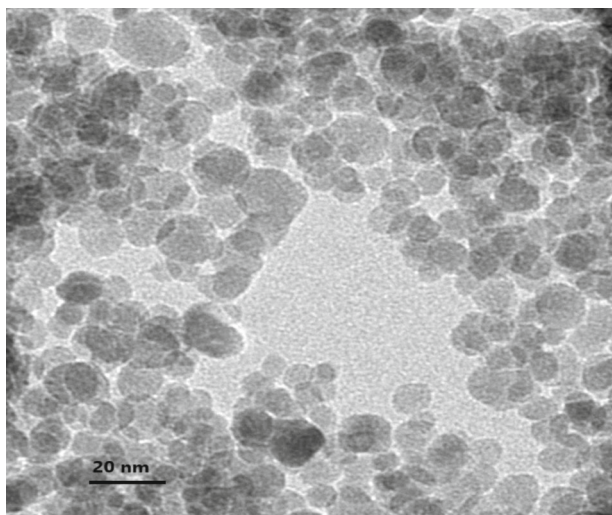
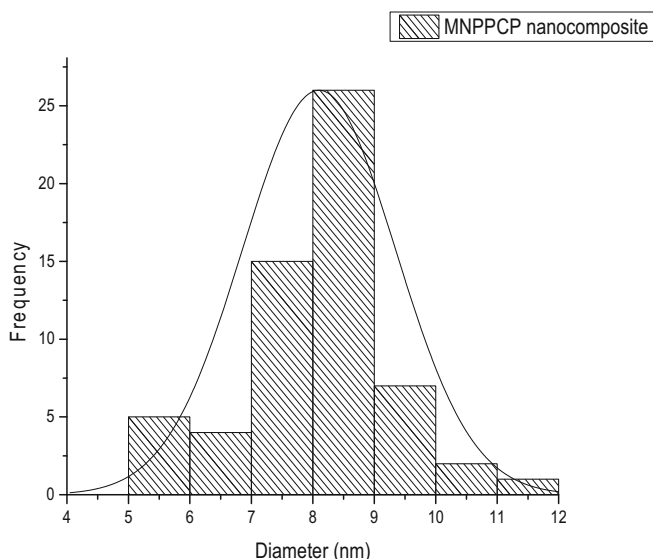


Fig. 1 TEM image and size distribution of MNP-PCP nanocomposite



on the surface of MNP-PCP. The distribution of the Fe atoms was like the O atoms as seen in Fig. 2d; this suggests that the Fe atoms are associated with the O atoms and the compound is likely iron oxide.

Effect of pH variation on As (III) uptake

Figure 3 shows the plots of total As, As (III), and change in H⁺ ion concentration for As (III) adsorption onto MNP-PCP in the pH range of 1 to 10. The results show rapid increase in the change in H⁺ ion concentration between solution pH 1 and 3 which then became constant from solution pH 4 to 10. The observed rapid change in H⁺ ion concentration at low pH was attributed to protonation of functional groups such as Fe-OH on the magnetite in MNP-PCP (Aryal et al. 2010). This was confirmed by running a blank sample in the absence of As (III) (plots not shown).

Total As and As (III) concentrations left in solution was observed to decrease with pH from pH 1 to 6 and decreased rapidly as solution pH was increased between 6 and 8 reaching a minimum at pH 8 and increased above pH. The speciation of As (III) in solution is known to vary depending on solution pH and at the pH range at which the experiments were performed (pH 1 to 10), As (III) species usually exist as H₃AsO₃ (pH < 2), H₂AsO₃ (pH 2 to 8), and H₃AsO₃⁻ (pH > 9) (Tian et al. 2011). At pH below 2, the total As and As (III) concentrations were quite high in solution due to the very weak binding of H₃AsO₃ to

the positive surface of adsorbents (Kamala et al. 2005). As solution pH was increased, the dominant form of As (III) became H₂AsO₃ and between pH 6 and 8, ligand exchange between As (III) and hydroxyl groups of Fe-OH in the coordination sphere of the surface (Zhang et al. 2015) was prevalent.



As solution pH rose above 9, As (III) exists as H₂AsO₃⁻ which is an anion which will experience electrostatic repulsion with the negative surfaces of the adsorbents thereby leading to increase in total and As (III) in solution (Tian et al. 2011).



Under low pH conditions, iron oxides are known to be slightly soluble in solution leaching out Fe (III). Fe (III) leached in solution is capable of oxidizing As (III) to As (V). Therefore, plots of concentration of Fe (III) and As (V) in solution versus the solution pH from 1 to 10 for MNP-PCP was made and shown in Fig. 3b. The results indicate that at pH 1, 2.33 mg/L of Fe (III) was leached out into solution. As the solution pH was increased to 6, the concentration Fe (III) leached reduced sharply owing to the decrease in H⁺ ions in solution. At solution pH 7, the Fe (III) leached was quite small and almost nondetectable up to pH 10. The presence of As (V) was noticed at solution pH of 1 and as pH increased to 6, the concentration of As (V) became very low and disappeared up to pH 10. This will explain the observed removal of As (III) from aqueous solution in the solution pH range between pH 2 and 4 through Fe (III) precipitation mechanism as shown:

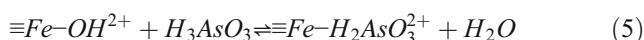
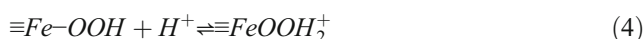
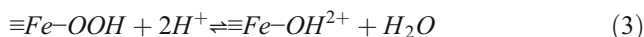


Table 1 Characteristics of MNP and MNP-PCP

Surface properties	MNP	MNP-PCP
BET surface area (m ² /g)	2.25	54.8
Pore volume (cm ³ /g)	0.0177	0.1522
Pore size (nm)	23.10	10.17

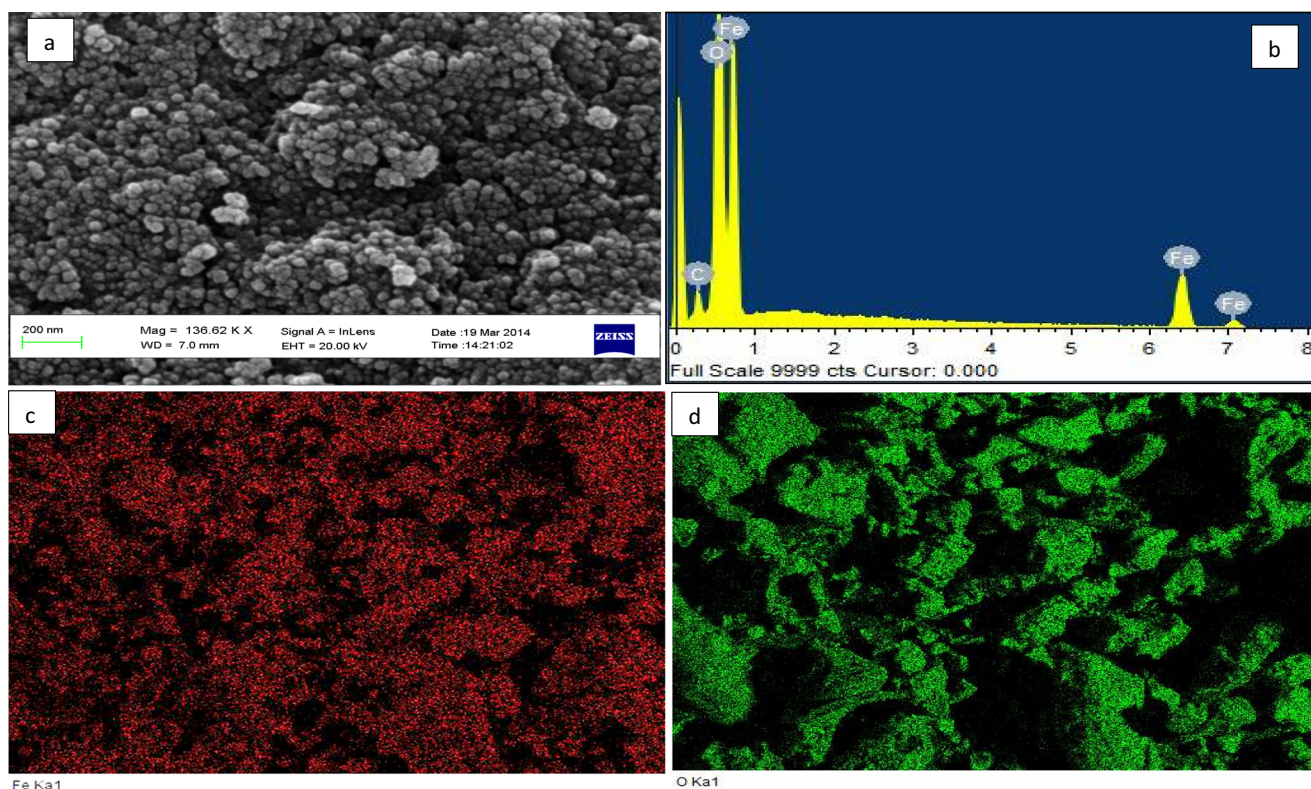


Fig. 2 **a** SEM image of MNP-PCP, **b** EDX analysis MNP-PCP, **c** Fe dispersion on MNP-PCP, and **d** O dispersion on MNP-PCP

Effect of pine to Fe_3O_4 ratio on As (III) removal

One aim of synthesizing adsorbent impact magnetic property on the final material while keeping the adsorption capacity maximum. Therefore, the preparation of MNP-PCP was carried out using varying pine cone masses (1.0 to 3.0 g) in the

coprecipitation reaction with fixed Fe (II)/Fe (III) masses and the composites produced were tested for their magnetic properties and ability to remove As (III) from aqueous solution. The synthesis of Fe_3O_4 in this process yields approximately 2.0 g of magnetite, therefore Fe_3O_4 :pine ratio in the products were approximately 2.0 g:1.0 g, 2.0 g:1.5 g, 2.0 g:2.0 g,

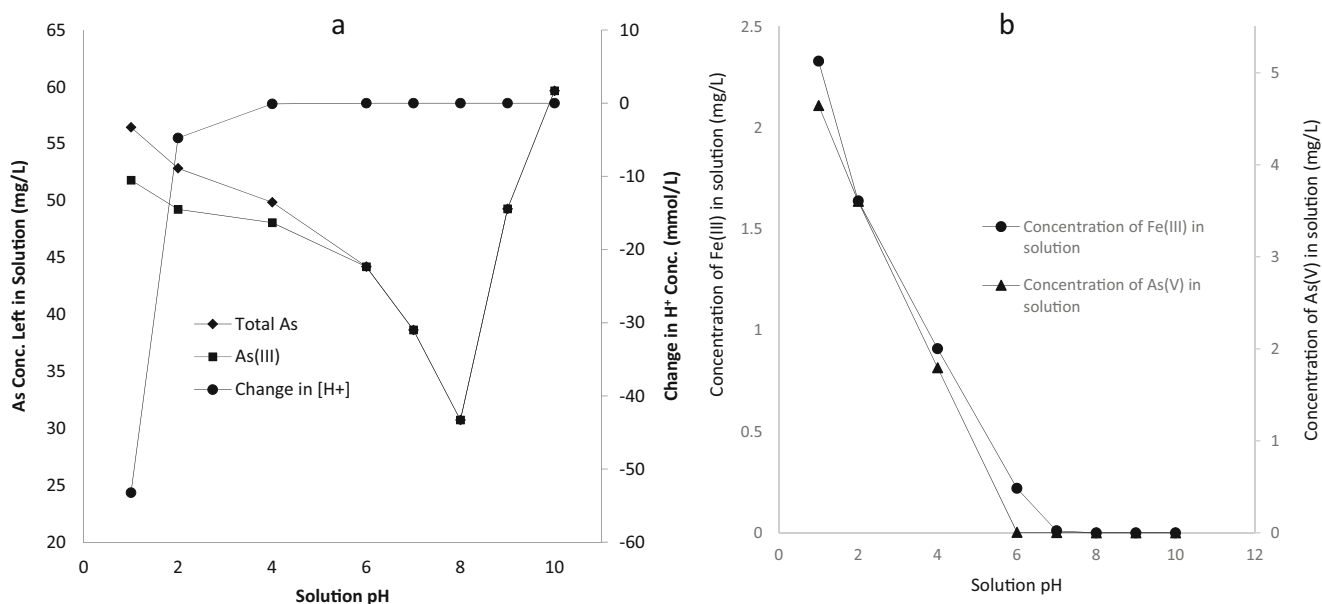


Fig. 3 **a** Effect of solution pH on total As and As (III) in solution in contact with MNP-PCP and **b** concentration of Fe (III) and As (V) left in solution at different solution pH's

2.0 g:2.5 g, and 2.0 g:3.0 g respectively, and As (III) capacity of the sample containing 1.0 g pine was 8.33 mg/g. Increment in the mass of pine in the composite to 0.15 g, the As (III) adsorption reached a maximum at 13.86 mg/g and further increment in mass of pine led to reduction in As (III) capacity to 8.48 mg/g when 3.0 g of pine cone was used.

The observed trend in the As (III) adsorption with increasing pine cone mass in the composite can be explained by looking at the SEM pictures of the various samples. Figure 4a–f shows the TEM images of bare MNP and MNP immobilized on different pine cone (PCP) masses from 0.1 to 3.0 g. Figure 4a shows the TEM of bare MNP which reveals that the particles are spherical and slightly agglomerated. The TEM micrograph of MNP on 1.0 g PCP is shown in Fig. 4b; the micrograph showed spherical shape for the magnetite nanoparticles which are closely packed on the surface of the biomass support. As the mass of pine cone was increased to 1.5 g (Fig. 4c), the spherical magnetite particles became better dispersed on the PCP support. The increase in dispersion of the nanoparticles on the support surface may account for the increase As (III) adsorption capacity. Cumbal and SenGupta (2005) reported that an increase in dispersion of hydrated iron oxide on an anion exchanger as substrate

improved arsenic adsorption. As the mass of PCP was increased to 2.0 g, it was observed that particle agglomeration increased (Fig. 4d). As the mass of PCP was increased from 2.0 to 2.5 and 3.0 g, agglomeration of magnetite nanoparticles increased and the PCP particles became visible in the TEM micrograph appearing as a separate phase (Fig. 4e, f).

The magnetic response of pure magnetite, PCP, and MNP-PCP with various masses of pine were measured using the applied field dependence of magnetization cycled between -15 and 15 kOe at room temperature and the values of saturation magnetization of the samples displayed in Table 2. The results show saturation magnetization for pure magnetite as prepared was 64.66 emu/g with the value of 92 emu/g for bulk Fe_3O_4 . The saturation magnetization values were least for PCP (2.47 emu/g) and increase from 34.34 to 37.50 emu/g in MNP-PCP with increase in PCP masses from 1.0 to 1.5 g. As the PCP mass was increased above 1.5 g, there was a reduction in saturation magnetization down to 17.15 emu/g at PCP mass of 3.0 g. Immobilization of MNP onto PCP was observed to reduce the saturation magnetism of magnetite but increased that of pine. The increase in saturation magnetism reached its optimum value with 1.5 g of pine.

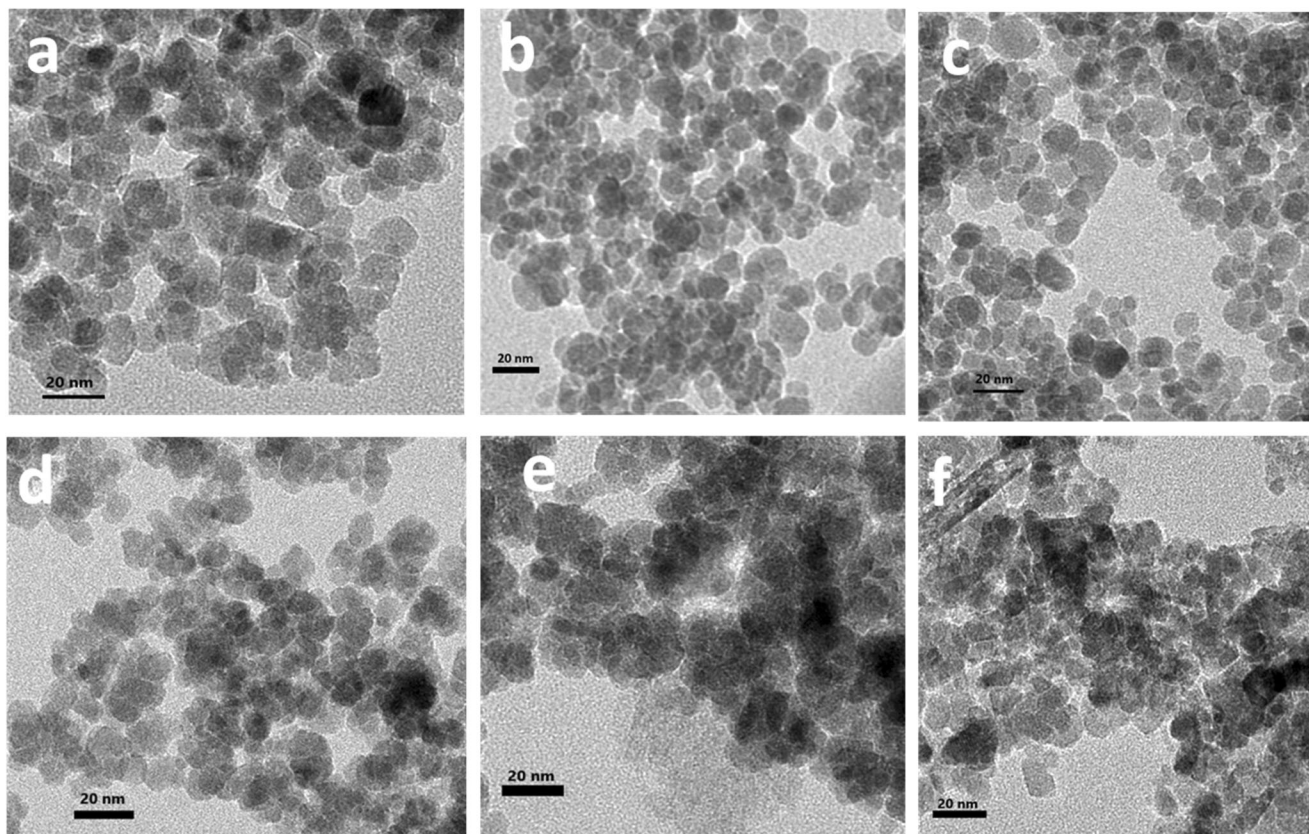


Fig. 4 TEM images of **a** MNP, **b** MNP immobilized on 1.0 g PCP, **c** MNP immobilized on 1.5 g PCP, **d** MNP immobilized on 2.0 g PCP, **e** MNP immobilized on 2.5 g PCP, and **f** MNP immobilized on 3.0 g PCP

Table 2 Adsorption capacities, saturation magnetization and coercivity MNP, and MNP immobilized on different masses of PCP

Sample	Adsorption capacity (mg/g)	Saturation magnetization (emu/g)	Coercivity (G)	Particle size (nm)
PCP	9.74	2.47	66.14	–
MNP	10.58	64.66	24.29	8.01
MNP on 1.0 g PCP	5.33	34.24	11.82	9.03
MNP on 1.5 g PCP	13.86	37.50	11.29	8.23
MNP on 2.0 g PCP	10.48	28.76	12.72	10.77
MNP on 2.5 g PCP	8.54	23.75	12.98	11.19
MNP on 3.0 g PCP	4.99	17.15	13.16	11.18

Temperature effect on As (III) kinetics

Adsorption kinetics of As (III) onto MNP-PCP was performed at different temperatures and the non-linear forms of the kinetic models in Eqs. (1) and (2) shown below:

$$q_t = q_e(1 - e^{-k_1 t}) \quad (6)$$

$$q_t = \frac{k_2 q_e^2 t}{1 + k_2 q_e t} \quad (7)$$

where q_e (mg/g) is the equilibrium capacities per gram of adsorbent and k_1 (min^{-1}) and k_2 (g/mg min) are the model rate constants. The results in Table 3 show the error determination as measured by correlation coefficient, r^2 and % variable error for

As (III). Error measurements for pseudo-first-order model were $r^2 > 0.95$ and % variable error < 290 while for pseudo-second-order, $r^2 > 0.996$ and % variable error < 25 . The pseudo-second-order model was observed to best describe the adsorption of As (III) better than the pseudo-first-order model. The plot of predicted adsorption capacities for each model against the experimental data were done to confirm the fit of this model to the experimental data (Supplementary Fig. S1). The rate constant, k_2 and initial sorption rates, h increased with temperature. The increase in As (III) capacity, k_2 , and h with temperature can be linked to increased mobility of As (III) ions in solution with increasing temperature and the larger surface area (Karthick et al. 2017). Increasing As (III) capacity with temperature also suggests that the adsorption process is endothermic.

Table 3 Kinetic data for As (III) adsorption onto MNP-PCP

Kinetic model	299 K	304 K	309 K	313 K	319 K
MNP-PCP					
Pseudo-first-order					
Model q (mg/g)	15.58	18.63	21.76	23.39	25.68
k_1 (min^{-1})	0.5013	0.6362	0.8636	0.0932	1.2957
r^2	0.9822	0.9506	0.9672	0.9573	0.9654
% Variable error	65.13	99.64	217.35	290.33	278.88
Pseudo-second-order					
Model q (mg/g)	16.74	19.58	22.33	24.62	27.01
k_2 ((g/mgmin)	0.0451	0.0512	0.0636	0.0726	0.0789
h (mg/g min)	12.638	19.629	31.713	44.006	57.561
r^2	0.9975	0.9964	0.9962	0.9966	0.9979
Variable error	7.52	16.58	24.63	25.19	16.69
Intraparticle diffusion model					
k_i ($\text{mg g}^{-1} \text{min}^{-0.5}$)	0.0998	0.0719	0.0518	0.0704	0.0689
C	15.529	18.542	21.720	23.960	26.357
r^2	0.9981	0.9715	0.9286	0.9997	0.9997
Film diffusion					
D_1 (cm^2/s)	2.22×10^{-14}	2.32×10^{-14}	2.38×10^{-14}	2.41×10^{-14}	2.48×10^{-14}
r^2	0.9477	0.9422	0.9776	0.9650	0.9304
Pore diffusion					
D_2 (cm^2/s)	1.59×10^{-13}	1.57×10^{-13}	1.43×10^{-13}	1.36×10^{-13}	1.32×10^{-13}
r^2	0.9681	0.9949	0.9938	0.9918	0.9783

The pseudo-second-order rate constant, k_2 was plotted using the Arrhenius expression as a function of temperature:

$$\ln k_2 = \ln k_0 - \frac{E_a}{RT} \tag{8}$$

where k_2 is the pseudo-second-order rate constant, k_0 is the temperature-independent factor, E_a is the activation energy of sorption (kJ/mol), R is the gas constant (8.314 J/mol K), and T is the solution temperature (K). E_a was then obtained from the slope of the plot of $\ln(k_2)$ versus $1/T$ and values. The plot was observed to be linear with r^2 of 0.9922 and activation energy of 23.78 kJ/mol. Heterogeneous reaction are known to have rate-limiting step that are controlled by chemical reaction at the surface or diffusion of the reactant (Lien and Zhang 2007). The activation energy of surface-controlled reactions in solutions are usually greater than 29 kJ/mol while the activation energies diffusion controlled reactions are usually between 8 and 21 kJ/mol (Karthick et al. 2017). The results of this study show activation energy in between 21 and 29 kJ/mol, meaning the rate-limiting step is complex, a mixture between surface and diffusion control. The activation energies of MNP-PCP were closer to diffusion controlled (23.78 kJ/mol).

Diffusion processes

Intraparticle diffusion

The proposed expression for the intraparticle diffusion of pollutant molecules into porous adsorbent given by Weber and Morris (1963) is:

$$q_t = k_p t^{0.5} + C \tag{9}$$

where C is the boundary layer effect or surface adsorption in the rate-determining step, k_p is the intraparticle diffusion rate constant, and q_t is the amount of As (III) adsorbed per unit mass at any time. An initial rapid section was observed in the plot of q_t versus $t^{0.5}$ (Supplementary Fig. S2) followed by slower stage in which As (III) uptake was almost constant. The plot of q_t versus $t^{0.5}$ did not yield a straight line passing through the origin indicating that intraparticle diffusion was not solely rate-limiting. The pattern of the line of the plots suggests that both film and particle diffusion influences As (II) adsorption (Banerjee and Chattopadhyaya 2017). The results in Table 3 revealed that the value of k_p decreased with temperature. The decreasing value of k_p with temperature is attributed to rapid surface reaction with increasing temperature (Hao et al. 2014). The magnitude of the constant, C increased with temperature suggesting greater participation of surface adsorption in MNP-PCP and activation of adsorption sites with increase in temperature.

Film and pore diffusion

It is accepted that film diffusion is predominant when external transport becomes greater than internal transport while pore diffusion participates more when internal diffusion is greater than external diffusion (Mittal et al. 2007). To evaluate the extent of the participation of film and pore diffusion in the adsorption process, the adsorbent particle was assumed to be a sphere of radius “ a .” The diffusion will then follow the expression:

$$\frac{q_t}{q_e} = 6 \left(\frac{D_1}{a^2} \right)^{0.5} \left\{ \pi^{-0.5} + 2 \sum_{n=1}^{\infty} \text{ierfc} \frac{\pi a}{D t^{0.5}} \right\} - 3 \frac{D t}{a^2} \tag{10}$$

At shorter amount of times, D is replaced by D_1 and Eq. (10) reduces to

$$\frac{q_t}{q_e} = 6 \left(\frac{D_1}{a^2} \right)^{0.5} t^{0.5} \tag{11}$$

The plots of fractional uptake of As (III) onto MNP-PCP versus $t^{0.5}$ are shown in Supplementary Fig. S3. The plot can be separated into two sections which are the initial rapid period and a slow and almost constant stage which is similar to the intraparticle diffusion profile. The values of the film diffusion constant, D_1 at different temperatures were then calculated from the slope of the plot of q_t/q_e versus time and recorded in Table 3. For longer reaction times, the relation between weight uptake and diffusion equation becomes:

$$\frac{q_t}{q_e} = 1 - \frac{6}{\pi^2} \sum_{n=1}^{\infty} \frac{1}{n^2} \exp \left(\frac{-D n^2 \pi^2 t}{a^2} \right) \tag{12}$$

$$\left(1 - \frac{q_t}{q_e} \right) = \frac{6}{\pi^2} \exp \left(\frac{-D_2 \pi^2 t}{a^2} \right) \tag{13}$$

If $B = (D_2 \pi^2 / a^2)$, Eq. (13) can be simplified as:

$$\left(1 - \frac{q_t}{q_e} \right) = \frac{6}{\pi^2} \exp(-Bt) \tag{14}$$

$$Bt = -0.4997 - \ln \left(1 - \frac{q_t}{q_e} \right) \tag{15}$$

The value of Bt at different temperatures therefore can be calculated from Eq. (10) and then plotted against t for the different temperatures. These plots can be used to identify if the rate of As (III) adsorption onto MNP-PCP is controlled by external or pore diffusion. The plots in Supplementary Fig. S4 show that the line did not pass through the origin indicating external mass transfer is rate-limiting at the initial stages of the process. External mass transfer at the initial stage was stronger than internal mass transfer as seen from the closeness of the lines to the

intercept. The values of B at different temperatures were calculated and the pore diffusion coefficient, D_2 determined by the expression:

$$B = \pi^2 \frac{D_2}{a^2} \quad (16)$$

The values of film diffusion, D_1 and pore diffusion, D_2 coefficients at different temperatures were calculated and reported in Table 3. The coefficient of film diffusion, D_1 was observed to increase with increasing temperature.

The increasing values of D_1 with temperature were due to increase in the mobility of As (III) ions due to retarding forces acting on the As (III) diffusion (Banerjee and Chattopadhyaya 2017). Santra and Sarkar (2016) also observed an increase in D_1 with temperature in the adsorption of As onto Cerium oxide loaded cellulose nanoparticle beads. The values of pore diffusion coefficients D_2 are shown in Tables 3. The reducing values of D_2 with increasing temperature and the reduction of D_2 with temperature can be attributed to increased surface reaction as temperature is increased.

Isotherm studies

A description of the adsorption type and the relationship between adsorbate in solution and adsorbate on the adsorbent surface at a given temperature was performed using the Langmuir, Freundlich, and Dubinin-Radushkevish (D-R) isotherm models. The non-linear expression of the Langmuir and Freundlich isotherm models is given as:

$$q_e = \frac{q_m K_a C_e}{1 + K_a C_e} \quad (17)$$

$$q_t = K_F C_e^{1/n} \quad (18)$$

$$q_e = q_s \exp(-\beta \varepsilon^2) \quad (19)$$

where q_e , q_s , and C_e represents the amount of As (III) adsorbed per unit mass of adsorbent (mg/g), the theoretical saturation capacity of the adsorbent (mol/g), and the equilibrium concentration of As (III) in solution (mg/L). The constants q_m and K_a represents the Langmuir monolayer capacity and the equilibrium constant, while the Freundlich constants K_F and n are related to adsorption capacity and intensity. The D-R isotherm constants β (mol^2/kJ^2) indicates the adsorption energy and ε the polyani potential. The polyani potential can be obtained from the expression:

$$\varepsilon = RT \ln \left[1 + \frac{1}{C_e} \right] \quad (20)$$

where T is the kelvin temperature (K) and R is the universal gas constant ($8.314 \text{ J mol}^{-1} \text{ K}^{-1}$). The mean free energy of adsorption, E , which is defined as the energy change

required for transferring a mole of adsorbate from solution to the adsorbent surface is expressed as:

$$E = \frac{1}{\sqrt{2\beta}} \quad (21)$$

The value of E gives information on whether the adsorption mechanism is physical, ion-exchange, or chemical.

The values of the Langmuir, Freundlich, and D-R isotherm constants along with the error determination using the coefficient of determination r^2 and the %variable error are shown in Table 4. The results revealed that the r^2 values were higher for the Langmuir isotherm while the % variable error was lower. This shows that the Langmuir isotherm gave better fit to the uptake of As (III) onto MNP-PCP and the adsorption was monolayer in nature with homogeneous adsorbent sites having uniform energy.

The adsorption efficiency of the MNP-PCP can be determined using the dimensionless constant separation factor for the equilibrium parameter (R_L), calculated using the expression:

$$R_L = \frac{1}{1 + K_a C_0} \quad (22)$$

where K_a (L/mg) and C_0 (mg/L) are the Langmuir equilibrium constant and the initial As (III) concentration. When the value of R_L is less than 1, the adsorption is favorable; when R_L is greater than 1, the adsorption is unfavorable; when R_L equals 0, the adsorption is irreversible; and when R_L equals 1, it is linear. The results in Table 4 show that the R_L values were in the range of 0.0349 to 0.0040 as temperature increased from 299 to 319 K. This suggests that adsorption of As (III) were favorable at all temperatures. Table 4 also shows that the r^2 (0.9979 to 0.9987) and % variable (7.68 to 8.55) values for D-R isotherm where high and therefore describe the isotherm data well. The theoretical saturation capacity q_s was observed to increase with increase in temperature while the adsorption energy β decreased with temperature from 299 to 319 K. The mean free energy of adsorption, E , had increased with temperature and had values between 12.13 and 15.30 kJ/mol which suggests ion-exchange process (Lunge et al. 2014). The As (III) adsorption capacity was compared favorable with those of other magnetic adsorbents as shown in Table 5.

Thermodynamics of As (III) adsorption onto MNP-PCP

The thermodynamics of As (III) adsorption onto MNP-PCP was determined using the expressions below:

$$\Delta G = -RT \ln K_a \quad (23)$$

$$\ln K_a = \frac{\Delta S}{R} - \frac{\Delta H}{RT} \quad (24)$$

Table 4 Equilibrium data for As (III) adsorption onto MNP-PCP

Isotherm model	26 °C	31 °C	36 °C	41 °C	46 °C
MNP-PCP					
Langmuir					
<i>q</i> (mg/g)	18.02	20.53	22.11	24.04	26.98
<i>K_a</i> (dm ³ /mg)	0.1845	0.3587	0.6382	0.8881	1.6673
<i>r</i> ²	0.9991	0.9960	0.9991	0.9992	0.9964
% Variable error	4.21	26.99	7.18	7.66	41.15
Separation factor	0.0349	0.0183	0.0103	0.0075	.00040
Freundlich					
<i>n</i>	3.57	4.01	4.28	4.40	4.49
<i>K_F</i> (mg/g) (dm ³ /mg) ^{1/<i>n</i>}	5.508	7.840	9.763	11.435	14.730
<i>r</i> ²	0.9591	0.9372	0.9466	0.9227	0.9089
% Variable error	195.82	419.07	434.56	729.52	1042.88
Dubinin–Radushkevich					
<i>q_s</i> (mol/g)	2.54 × 10 ⁻⁴	2.89 × 10 ⁻⁴	3.39 × 10 ⁻⁴	3.63 × 10 ⁻⁴	3.74 × 10 ⁻⁴
<i>β</i> (mol ² /J ²)	3.31 × 10 ⁻⁹	2.88 × 10 ⁻⁹	2.42 × 10 ⁻⁹	2.33 × 10 ⁻⁹	2.14 × 10 ⁻⁹
<i>E</i> (kJ/mol)	12.13	13.30	14.40	14.60	15.30
<i>r</i> ²	0.9987	0.9980	0.9979	0.9985	0.9981
% Variable error	7.76	7.68	7.88	8.07	8.55

where *R* is the universal gas constant (8.314 J/mol K), *T* is temperature (K), and *K_a* is the equilibrium constant of the Langmuir equation. The enthalpy (ΔH) and entropy (ΔS) parameters were estimated from the following equation. The values of ΔH and ΔS parameters can be calculated from the slope and intercept of the plot of $\ln K_a$ versus $1/T$. The calculated values of free energy, ΔG , ranged from -23.7 to -31.1 kJ/mol with increasing solution temperature (Table 6). The results show that the values of ΔG for MNP-PCP were negative at all temperatures indicating the thermodynamic feasibility and spontaneous nature of the adsorption. The adsorption process being feasible means that the adsorptive forces were able to overcome the potential barrier. The values of ΔH for MNP-PCP were calculated to be 84.27 kJ/mol, suggesting that the adsorption process is endothermic in nature at the reaction temperatures investigated. The values of ΔS for MNP-PCP were calculated to be 361.57 J/mol K indicating a release of orderly structured hydration water and increase in

the randomness at the solid/solution interface during the adsorption process (Meng et al. 2017).

Effect of ionic strength

The results show that As (III) adsorption capacity was higher at pH 8 when As (III) is in its neutral form and the adsorbent surface is relatively neutral with no added electrolyte (Fig. 5). Renkou et al. (Renkou et al. 2009) also reported higher adsorption of As (III) ions in soils rich with iron oxide at near neutral pH, but with lower capacities at low and high pH's. On addition of electrolyte, there was a slight increase in the As (III) capacity which increased with increasing ionic strength at the three pHs (Fig. 5). The increase can be attributed to the fact that ionic strength can compress the double layer making the electrostatic potential which contributes to adsorption became more positive, therefore increasing As (III) uptake (Chang et al. 2009). Therefore, as the ionic strength is

Table 5 Comparison of As (III) adsorption capacity onto different adsorbents

Adsorbents	Conc. (mg/dm ³)	pH	Dose	Adsorption capacity	Reference
Magnetic wheat straw	1–28 mg/dm ³	8	5.0 g/dm ³	3.90 mg/g	[19]
Iron/Olivine composite	1–10 mg/dm ³	7	3.0 g/dm ³	2.83 mg/g	[23]
Fe (III)-treated <i>Staphylococcus xylosus</i>	10–300 mg/dm ³	7	3.0 g/dm ³	5.93 mg/g	[18]
Iron oxide coated seed	1–40 mg/dm ³	7	10.0 g/dm ³	4.00 mg/g	[32]
Magnetite-reduced graphene oxide	3–7 mg/dm ³	7	0.2 g/dm ³	13.01 mg/g	[23]
MNP-PCP	25–150 mg/dm ³	8	5.0 g/dm ³	13.86 mg/g	This study

Table 6 Thermodynamics parameters of As (III) adsorption onto PCP and MNP-PCP

Adsorbent	Temperature (K)	ΔG (kJ/mol)	ΔH (kJ/mol)	ΔS (J/mol K)
PCP	299	-22.2	81.34	347.19
	301	-24.6		
	309	-25.9		
	314	-27.6		
	319	-29.7		
MNP-PCP	299	-23.7	84.27	361.57
	301	-25.8		
	309	-27.7		
	314	-29.0		
	319	-31.1		

increased, As (III) adsorption capacity increases slightly. The increase As (III) capacity was 22.22% when NaNO_3 of concentration 0.02 mol/L was applied. Yu et al. (2015) observed a slight increase in capacity with ionic strength when the authors increased ionic strength of the solution in the adsorption of As (III) onto magnetic graphene oxide.

Effect of competing anions

The effect of competing anions, SO_4^{2-} , CO_3^{2-} , PO_4^{3-} and Cl^- , on the adsorption of As (III) onto MNP-PCP at pH 6, 8 and 10 are shown in Fig. 6. The results show that the presence of SO_4^{2-} , CO_3^{2-} and Cl^- in the solution had slight positive influence on the adsorption of As (III) onto MNP-PCP. The magnitude of the increase was in the order of $\text{Cl}^- > \text{SO}_4^{2-} > \text{CO}_3^{2-}$.

The reason for this slight increase in As (III) uptake can be linked to the fact that binding affinities of SO_4^{2-} , CO_3^{2-} and Cl^- are much weaker than that of As (III) (Yu et al. 2013). Chang et al. (2009) also observed a slight increase in As (III) adsorption

onto Fe–Mn binary oxide when the adsorption process was performed in the presence of SO_4^{2-} and CO_3^{2-} at solution pH of 3.5, 6.0, and 9.0. Adsorption in the presence of PO_4^{3-} anions reduced As (III) adsorption and the effect was stronger at higher solution pH. Similar observation was made by Yu et al. (2013) and Sahu et al. (2017) in the adsorption of As (III) onto cellulose@iron oxide nanoparticles and cigarette soot activated carbon modified with Fe_3O_4 nanoparticles. The reduction in As (III) adsorption is thought to arise from the fact that PO_4^{3-} forms much stronger bonds than As (III) with the adsorbents since it shares similar chemical characteristics as arsenic (Wu et al. 2013). Therefore, by the mechanisms such as competitive adsorption and charge diffusion, PO_4^{3-} is able to reduce drastically the adsorption of As (III) from solution (Goldberg 2002).

Effect of humic acid

The effect of the presence of humic acid on the uptake of As (III) onto MNP-PCP with respect to humic acid concentration

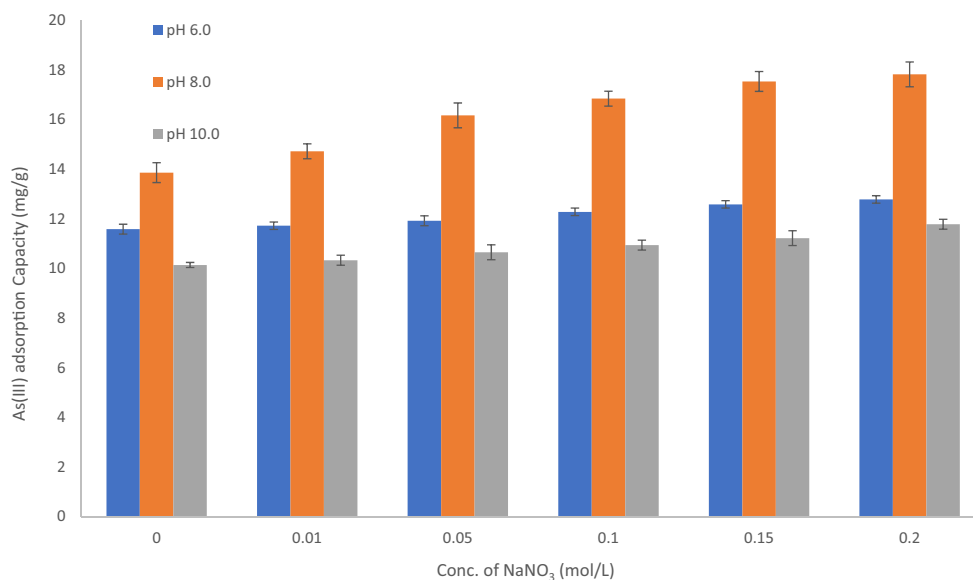
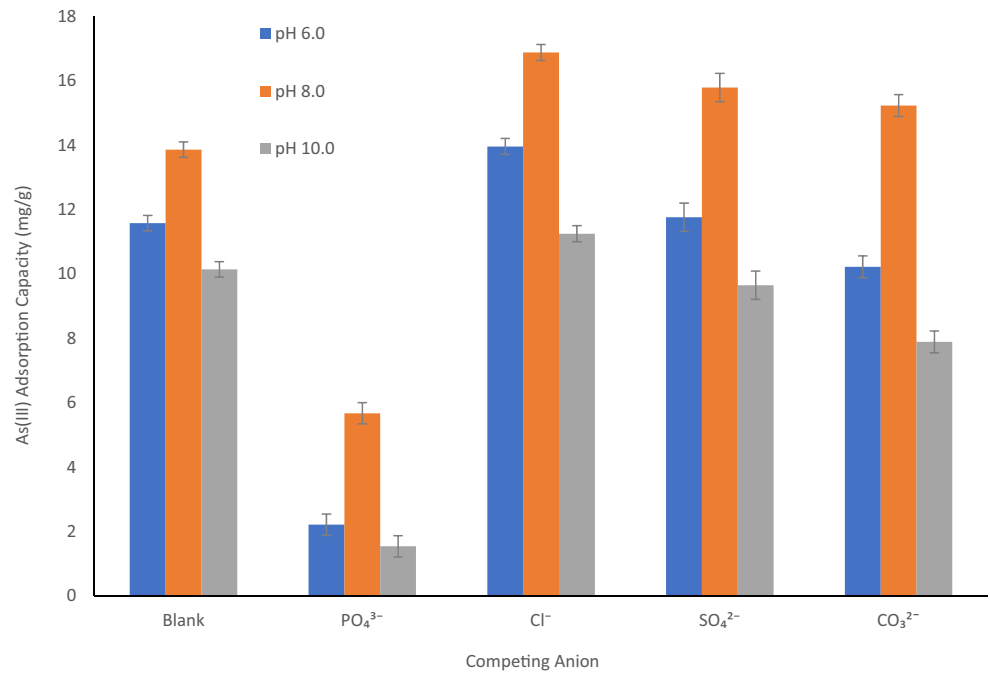
Fig. 5 Effect of NaNO_3 ionic strength at different initial solution pH on the adsorption of As (III) onto MNP-PCP nanocomposite

Fig. 6 Effect of competing ions on the adsorption of As (III) onto MNP-PCP nanocomposite

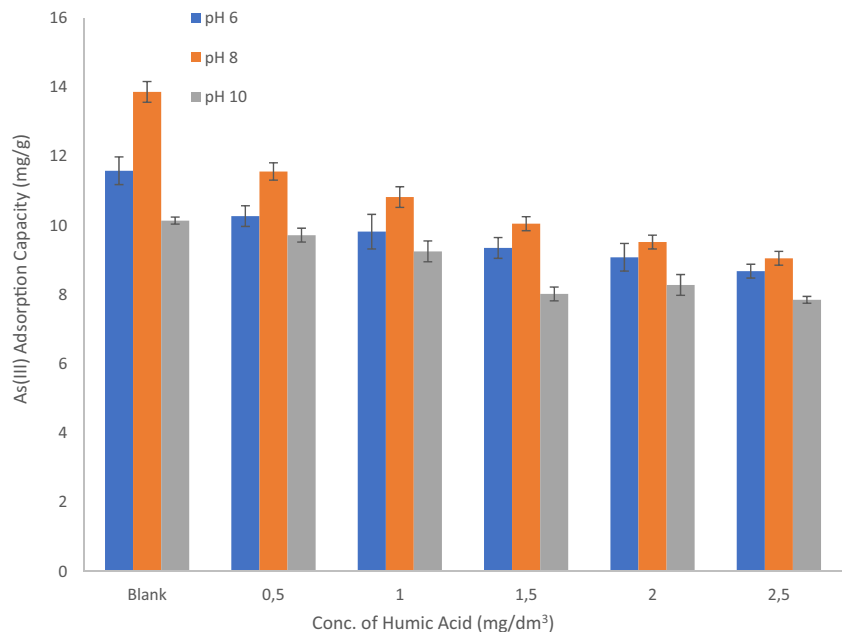


and solution pH is shown in Fig. 7. The results in Fig. 7 show that As (III) uptake onto MNP-PCP decreased in the presence of humic acid at all solution pH's and the extent of reduction was observed to be high at solution pH around 6. Humic acids are known to contain a variety of acidic functional groups such as hydroxyl, carboxylic, and phenolic groups and the presence of these groups gives humic acids high affinity for magnetite particles (Liu et al. 2008). Therefore, humic acids usually interact with magnetite nanoparticles to form aggregates (Aaron et al. 2002) and promote the occupation of adsorption sites on the magnetite surface leading to reduction in the number of active sites for As (III)

bonding (Giasuddin et al. 2007). The above reasons may therefore account for the reduction in As (III) adsorption on addition of humic acid to the solution. With increasing concentration of humic acids in the solution, the reduction in As (III) adsorption was observed to increase. This suggests that interaction between humic acid and MNP-PCP increased as humic acid concentration was increased. It has also been reported that the presence of humic acids in solution slows down the rate at which As (III) ions accesses favorable binding sites on magnetite particles (Giasuddin et al. 2007).

The charge on both MNP-PCP and As (III) can be affected by solution pH, for examples As (III) can exist as

Fig. 7 Effect of humic acid on the adsorption of As (III) onto MNP-PCP



H_3AsO_3 at $pH < 2$, H_2AsO_3 between $pH 6$ and 8 , and $H_2AsO_3^-$ above $pH 9$ (Zhang et al. 2015). Humic acids usually become increasingly positively charged as solution pH decreases from their point zero charge of $pH 7.7$ (Kanel et al. 2006). Therefore, at low solution pH , both humic acid and magnetite surface are positively charged and As (III) species (H_3AsO_3) is not strongly attracted to humic acids or magnetite, therefore the influence of humic acids on As (III) adsorption is low. At higher solution pH 's, humic acid, magnetite surface, and As (III) species ($H_2AsO_3^-$) are all negatively charged, therefore adsorption and competition for As (III) is also low. Around solution $pH 8$, humic acid, magnetite surface, and As (III) species ($H_2AsO_3^-$) are predominantly neutral, therefore adsorption and competition is maximum. This explains the higher reduction in As (III) capacity at $pH 8$ and the lower reduction and competition at lower and higher pH 's. Comparable results have been reported by Aaron et al. (2002).

Adsorption mechanism

Several results obtained from these experiments points to the probable mechanism of As (III) adsorption onto MNP-PCP. These results include (1) the higher As (III) removal capacity at solution pH of 8 at which both the predominant arsenic species and the surface charge on the adsorbent were close or actually neutral, (2) the value of the Dubinin-Radushkevich mean free energy E which was in the range of 8 and 16 kJ/mol, and (3) the slight increase in As (III) adsorption capacity with ionic strength at different pH 's which suggests ligand ion-exchange mechanism. Therefore, to confirm this mechanism, (i) the FTIR spectra before and after As (III) adsorption, (ii)

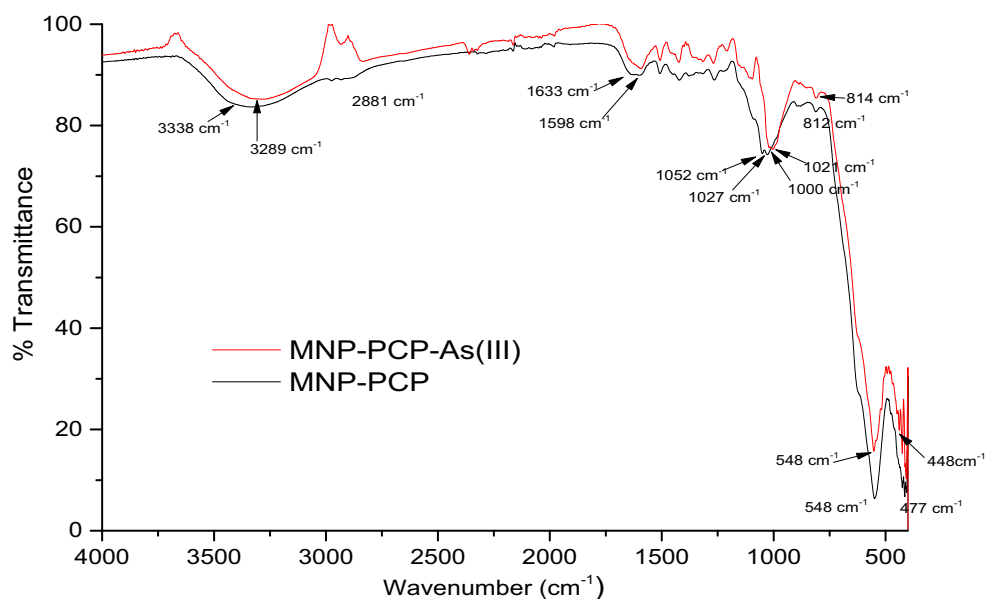
XPS before and after As (III) adsorption, and (iii) point zero charge before and after As (III) adsorption and the displacement of adsorbed nitrate ions were performed.

Figure 8 shows the FTIR spectrum of MNP-PCP before and after As (III) adsorption. The spectrum shows peaks at 3338 , 2881 , 1633 , 1598 , and 1052 cm^{-1} representing hydrogen bond stretching of α -cellulose, methylene $-CH_3$, $-CH_2-$, of cellulose (Subramanian et al. 2005), and $C=O$, $C-O$, $C-O-C$ in lignin (Gupta and Nayak 2012b). The peaks at 1027 , 548 , and 477 cm^{-1} are attributed to $Fe-O$ and $Fe-OH$ (Reza and Ahmaruzzaman 2015) groups in MNP-PCP. After As (III) adsorption, reduction and shift in peak intensities were observed for $-OH$ stretching of α -cellulose from 3338 to 3289 cm^{-1} , the $C-O-C$ and $Fe-O$ from 1052 and 1027 to 1021 and 1000 cm^{-1} , and $Fe-OH$ peak from 477 to 448 cm^{-1} . The shift in peak at 812 to 814 cm^{-1} has been attributed to the formation of $As-O$ bond (Meng et al. 2017). Several authors have concluded that this shift in peaks of oxygenated groups and especially to the peak at 814 cm^{-1} accounts for the formation of $As-O$ bonds (Meng et al. 2017; Venkatesan and Narayanan 2018).

To confirm the presence of the formation of $As-O$ bond, the XPS analysis of MNP-PCP before and after As (III) adsorption was performed and results were shown in Fig. 9a–h. XPS survey spectra of MNP-PCP before and after As (III) adsorption in Fig. 9a, b shows three major peaks at binding energies 284 , 530 , and 710 eV corresponding to $C 1s$, $O 1s$, and $Fe 2p$ photoemissions, respectively. The spectrum for MNP-PCP after As (III) adsorption was observed to have a new peak at binding energy 43.5 eV corresponding to As (III) $3d$ (Mahanta and Chen 2013).

The $Fe 2p$ spectrum before and after As (III) adsorption are shown in Fig. 9c, d. Figure 9a shows two strong peaks at

Fig. 8 FTIR spectra of MNP-PCP before and after As (III) adsorption



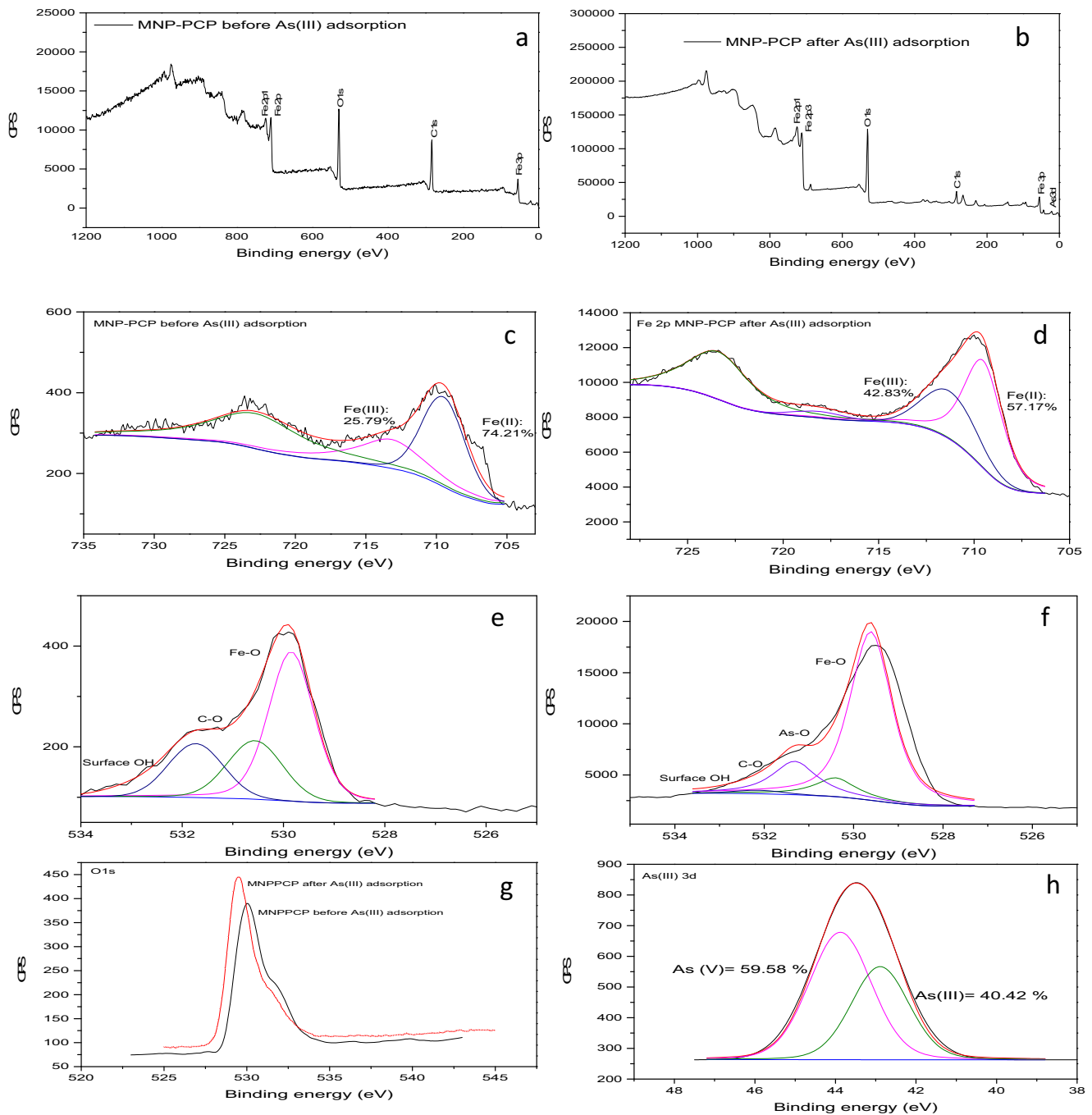


Fig. 9 Full spectra of MNP-PCP **a** before As (III) adsorption and **b** after As (III) adsorption. Fe 2p spectra of MNP-PCP **c** before As (III) adsorption and **d** after As (III) adsorption. O 1s spectra of MNP-PCP **e** before As

(III) adsorption and **f** after As (III) adsorption. **g** O 1s spectra of MNP-PCP before and after As (III) adsorption. **h** As3d spectra of MNP-PCP after As (III) adsorption

binding energies of 709.9 and 723.5 eV corresponding to Fe 2p_{3/2} and Fe 2p_{1/2}, respectively, which can be attributed to magnetite (Yoon et al. 2017). The peak at binding energy of 709.9 eV before and after As (III) adsorption was curve fitted into two peaks with binding energies at 709.73 and 713.48 eV, assigned to Fe (II) and Fe (III), respectively (Wilson and Langell 2014). The % atomic concentration of Fe (II) and Fe (III) on the MNP-PCP before adsorption was 74.2% Fe (II)

and 25.8% Fe (III), while after adsorption was 57.2% Fe (II) and 42.8% for Fe (III) respectively indicating that Fe (II) was partially oxidized to Fe (III).

The O 1s spectrum of the MNP-PCP adsorbent before As (III) adsorption (Fig. 9e, f) is composed of three component peaks at 530.56, 531.73, and 532.71 eV, which are respectively assigned to the Fe-O, the C-O group, and the adsorbed water (H₂O). The presence of the As-O peak after As (III)

Table 7 Parameters for As (III)/NO₃⁻ exchange processes

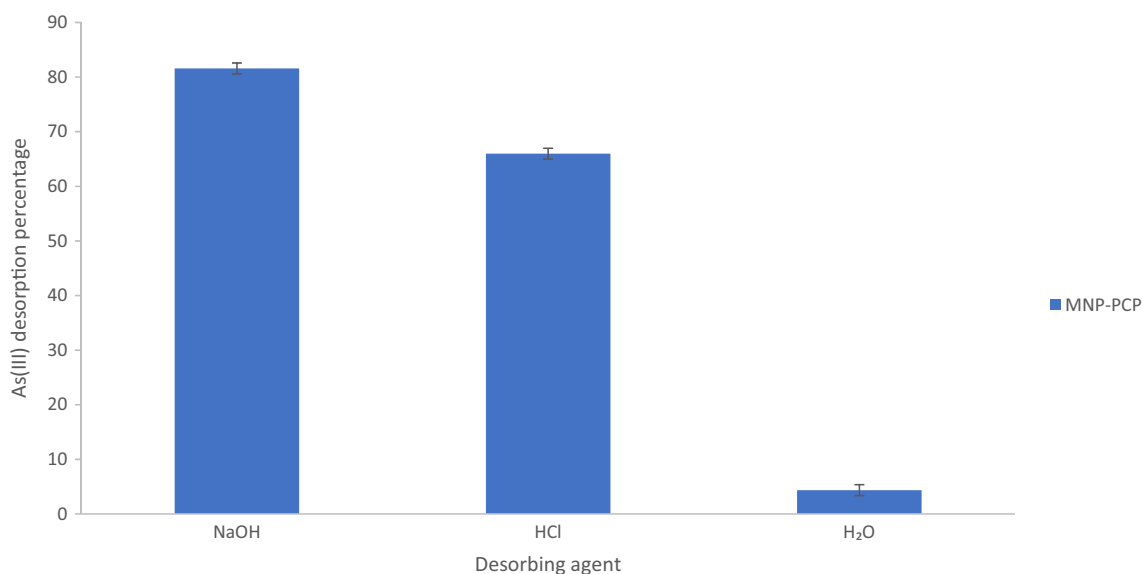
As (III) Init. Conc. (mg/dm ³)	Amt. of NO ₃ ⁻ released (mol/g)	As (III) adsorbed (mol/g)	As (III)/NO ₃ ⁻ exchange coefficient ($R_{As(III)/NO_3^-}$)
0	0.00	0.00	0.00
5	0.474117	0.054378	0.114693
25	0.627318	0.141324	0.225283
50	0.683761	0.304925	0.445953
100	0.849863	0.631741	0.743344

adsorption (Fig. 9f) confirms the As (III) adsorption onto MNP-PCP surface (Yu et al. 2013; Zhang et al. 2010). The surface hydroxyl peak and the carbonyl peak reduced after As (III) adsorption, indicating the decrease in the amount of hydroxyl group on the adsorbent surface during arsenic adsorption. The results also show that there was a shift in the O 1s peak before and after As (III) adsorption (Fig. 9g). The XPS spectrum of As (III) 3d (Fig. 9h) was observed to be composed of two characteristic peaks with binding energies of 42.9 and 43.9 eV with % concentration on 57.17 and 42.8% corresponding to As (III) and As (V), respectively.

The experimental results of this study show a slight increase in adsorption capacity with ionic strength which has been attributed to increased activity of the counter ions which compensates surface charge due to specific ion adsorption. The author then used pH_{PZC} analysis to differentiate between inner sphere and outer sphere complex ligand formation. Goldberg and Johnston (2001) reported the shift in the value of pH_{PZC} due to arsenite adsorption onto surfaces as evidence of strong specific ion adsorption brought about by inner sphere complex formation. Therefore in this study, the pH_{PZC} of MNP-PCP before and after As (III) adsorption was determined and is shown in Supplementary Fig. S5. The pH_{PZC} values obtained were 5.86 and 4.26 for MNP-PCP and MNP-PCP-As (III)

respectively. The results show that there was a reduction in pH_{PZC} when As (III) was adsorbed on the surface of MNP-PCP. This suggests that As (III) adsorption formed a negatively charged inner sphere complex on MNP-PCP surface (Pena et al. 2006). The formation of a negatively charged inner sphere complex can either be due to deprotonation of H₃AsO₃ on the surface of MNP-PCP (Pena et al. 2006) or the oxidation of As (III) to As (V) on the MNP-PCP surface (Lakshmiathiraj et al. 2006). It was observed from the experiments in “Diffusion processes” section that at solution pH 8, the presence of As (V) was not detected in solution. From the XPS spectrum of As (III) 3d, it was observed that both As (III) and As (V) were present in % concentration on 57.17 and 42.8% respectively, therefore the negatively charged As (III) inner sphere complex on MNP-PCP surface can be attributed to oxidation reaction of As (III) to As (V) on MNP-PCP surface (Zhao et al. 2011).

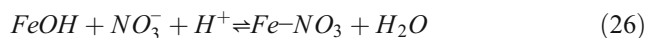
To confirm ion-exchange process as the adsorption mechanism, NO₃⁻-loaded MNP-PCP was prepared by adsorbing NO₃⁻ ions onto MNP-PCP and washing to remove excess NO₃⁻ ions. Then, 0.1 g of the NO₃⁻-loaded MNP-PCP was then contacted with different concentrations (5, 25, 50, 100 mg/L) of As (III) solution. The amount of NO₃⁻ ions released and the As (III) adsorbed were estimated and the

**Fig. 10** Desorption studies for As (III) onto MNP-PCP

results recorded in Table 7. The results show an increase in NO_3^- ions released as the initial As (III) concentration and the As (III) capacity increases. This shows evidence of ligand exchange between the NO_3^- and the As (III) anions. Similarities between As (III) adsorbed and SO_4^{2-} released were made by Burton et al. (2009) and Wu et al. (2013) in the adsorption of As (III) onto Schwertmannite and Fe-based backwashing sludge respectively. Both authors studied the molar ratios of SO_4^{2-} released and As (III) adsorbed on Schwertmannite and Fe-based backwashing sludge defined as the As (III)/ SO_4^{2-} exchange coefficient ($R_{\text{As(III)}/\text{SO}_4^{2-}}$). The values of the exchange coefficients were 0.16 to 0.31 for Schwertmannite and 0.11 to 0.25 for Fe-based backwashing sludge. In this study, the exchange coefficient ($R_{\text{As(III)}/\text{NO}_3^-}$) was determined as the ratio of NO_3^- released to As (III) adsorbed. The values of exchange coefficient ($R_{\text{As(III)}/\text{NO}_3^-}$) ranged from 0.11 to 0.74 which was comparable to the results of Wu et al. (Wu et al. 2013). This suggested that NO_3^- ions exchanged were located within the tunnels of MNP-PCP and not just the surface adsorbed ones. A plot of the exchange coefficient values against the amount of As (III) left in solution gave a straight line with r^2 value of 0.9897 which can be represented by the relationship:

$$R_{\text{As(III)}/\text{NO}_3^-} = 0.0125C_{e_{\text{As(III)}}} + 0.0844 \quad (25)$$

Therefore, the reaction scheme can be written for the displacement of NO_3^- from NO_3^- -loaded by As (III) as shown:



These series of tests therefore confirm the presence of ligand anion-exchange reaction as the mechanism for As (III) adsorption onto MNP-PCP.

Desorption studies

To further investigate the binding mechanism of As (III) onto MNP-PCP, the desorption studies were conducted using 0.5 M of NaOH, HCl, and H_2O as the desorbing agent and the results are shown in Fig. 10. The results show that NaOH had the highest As (III) desorption percentage of 81.6%, followed by HCl (65.98%) and H_2O (4.35%). This suggests that ion-exchange is the main dominating mechanism for As (III) adsorption onto MNP-PCP while physical adsorption slightly contributed to the binding mechanism. Strong bases and acids have been reported to be the most common desorbing agents for arsenic. Zhou et al. (Zhou et al. 2014) desorbed 96.5% of As (III) from magnetic cellulose

nanocomposite using 0.1 M HCl while Yoon et al. (Yoon et al. 2017) desorbed 73.4% of As (III) from magnetite/non-oxidative graphene composite using 0.1 M NaOH. Both authors and the results obtained in this work confirm that the interaction between As (III) and magnetite-coated samples is due to ion-exchange mechanism.

Conclusion

Adsorption of As (III) onto magnetite nanoparticles coprecipitated on pine cone (1.0 g) was studied. Optimum adsorption conditions were pH 8 and adsorbent dose of 5 g/L. An increase was observed in the pseudo-second-order capacity and rate constant with temperature and was applied in the determination of activation energy. The rate-limiting step was a mixed process of surface and pore control. Both the Langmuir and D-R isotherm showed that adsorption process was favorable at all temperatures, monolayer in nature and a ligand exchange process. FTIR evidence of ligand exchanged was observed as shifts in peaks at 814 cm^{-1} representing As-O bonding. XPS confirms the formation As-O bonding as well as absence of As (V) at pH 8 and the presence of As (V) in the matrix of the spent adsorbent suggests the oxidation of As (III) adsorbed on MNP-PCP. The lowering of pH_{PZC} with As (III) adsorption and the trend in the displacement of NO_3^- from NO_3^- -loaded MNP-PCP with increasing concentrations of As (III) along with the values of anion-exchange coefficient confirms ligand ion exchange as the reaction mechanism.

References

- Aaron DR, Macalady DL, Ahmann D (2002) Natural Organic Matter Affects Arsenic Speciation and Sorption onto Hematite. *Environ Sci Technol* 36:2889–2896
- Amin MN, Kaneco S, Kitagawa T, Begum A, Katsumata H, Suzuki T, Ohta K (2006) Removal of arsenic in aqueous solutions by adsorption onto waste rice husk. *Ind Eng Chem Res* 45:8105–8110
- Ansone L, Klavins M, Viksna A (2013) Arsenic removal using natural biomaterial-based sorbents. *Environ Geochem Health* 35:633–642
- Aryal M, Ziagova M, Liakopoulou-Kyriakides M (2010) Study on arsenic biosorption using Fe (III)-treated biomass of *Staphylococcus xylosus*. *Chem Eng J* 162:178–185
- Banerjee S, Chattopadhyaya M (2017) Adsorption characteristics for the removal of a toxic dye, tartrazine from aqueous solutions by a low cost agricultural by-product. *Arab J Chem* 10:S1629–S1638
- Biswas BK, Inoue J-i, Inoue K, Ghimire KN, Harada H, Ohto K, Kawakita H (2008) Adsorptive removal of As (V) and As (III) from water by a Zr (IV)-loaded orange waste gel. *J Hazard Mater* 154: 1066–1074
- Burton ED, Bush RT, Johnston SG, Watling KM, Hocking RK, Sullivan LA, Parker GK (2009) Sorption of arsenic (V) and arsenic (III) to schwertmannite. *Environ. Sci. Technol.* 43:9202–9207

- Chang F, Qu J, Liu H, Liu R, Zhao X (2009) Fe–Mn binary oxide incorporated into diatomite as an adsorbent for arsenite removal: preparation and evaluation. *J Colloid Interface Sci* 338:353–358
- Chung J-Y, Yu S-D, Hong Y-S (2014) Environmental source of arsenic exposure. *J Prev Medi Public Health* 47:253–257
- Cumbal L, SenGupta AK (2005) Arsenic removal using polymer-supported hydrated iron (III) oxide nanoparticles: role of Donnan membrane effect. *Environ Sci Technol* 39:6508–6515
- Fang L, Ghimire KN, Kuriyama M, Inoue K, Makino K (2003) Removal of fluoride using some lanthanum (III)-loaded adsorbents with different functional groups and polymer matrices. *J Chem Technol Biotechnol* 78:1038–1047
- Giasuddin ABM, Kanel SR, Choi H (2007) Adsorption of Humic Acid onto Nanoscale Zerovalent Iron and Its Effect on Arsenic Removal. *Environ Sci Technol* 41:2022–2027
- Goldberg S, Johnston CT (2001) Mechanisms of arsenic adsorption on amorphous oxides evaluated using macroscopic measurements, vibrational spectroscopy, and surface complexation modeling. *J Colloid Interface Sci* 234:204–216
- Goldberg S (2002) Competitive adsorption of arsenate and arsenite on oxides and clay minerals. *Soil Sci Soc Am J* 66:413–421
- Goswami A, Raul P, Purkait M (2012) Arsenic adsorption using copper (II) oxide nanoparticles. *Chem Eng Res Des* 90:1387–1396
- Gupta V, Nayak A (2012a) Cadmium removal and recovery from aqueous solutions by novel adsorbents prepared from orange peel and Fe₂O₃ nanoparticles. *Chem Eng J* 180:81–90
- Gupta V, Nayak A (2012b) Cadmium removal and recovery from aqueous solutions by novel adsorbents prepared from orange peel and Fe₂O₃ nanoparticles. *Chem Eng J* 180:81–90
- Hao L, Ouyang T, Lai L, Liu Y-X, Chen S, Hu H, Chang C-T, Wang J-J (2014) Temperature effects on arsenate adsorption onto goethite and its preliminary application to arsenate removal from simulative geothermal water. *RSC Adv* 4:51984–51990
- Hua M, Yang B, Shan C, Zhang W, He S, Lv L, Pan B (2017) Simultaneous removal of As (V) and Cr (VI) from water by macroporous anion exchanger supported nanoscale hydrous ferric oxide composite. *Chemosphere* 171:126–133
- Kamala C, Chu K, Chary N, Pandey P, Ramesh S, Sastry A, Sekhar KC (2005) Removal of arsenic (III) from aqueous solutions using fresh and immobilized plant biomass. *Water Res* 39:2815–2826
- Kanel SR, Grenèche JM, Choi H (2006) Removal of arsenic (III) from groundwater using nano scale zero-valent iron. *Environ Sci Technol* 39:1291–1298
- Karthick K, Namasivayam C, Pragasan LA (2017) Removal of direct red 12B from aqueous medium by ZnCl₂ activated Jatropa husk carbon: adsorption dynamics and equilibrium studies. *Indian J Chem Technol* 24:73–81
- Kumar E, Bhatnagar A, Hogland W, Marques M, Sillanpää M (2014) Interaction of inorganic anions with iron-mineral adsorbents in aqueous media—a review. *Adv Colloid Interf Sci* 203:11–21
- Lakshmi pathiraj P, Narasimhan B, Prabhakar S, Raju GB (2006) Adsorption studies of arsenic on Mn-substituted iron oxyhydroxide. *J Colloid Interface Sci* 304:317–322
- Lien H-L, Zhang W-X (2007) Nanoscale Pd/Fe bimetallic particles: catalytic effects of palladium on hydrodechlorination. *Appl Catal B Environ* 77:110–116
- Liu J-F, Zhao Z-S, Jiang G-B (2008) Coating Fe₃O₄ Magnetic Nanoparticles with Humic Acid for High Efficient Removal of Heavy Metals in Water. *Environ Sci Technol* 42:6949–6954
- Lunge S, Singh S, Sinha A (2014) Magnetic iron oxide (Fe₃O₄) nanoparticles from tea waste for arsenic removal. *J Magn Magn Mater* 356:21–31
- Mahanta N, Chen JP (2013) A novel route to the engineering of zirconium immobilized nano-scale carbon for arsenate removal from water. *J Mater Chem A* 1:8636–8644
- Meng F, Yang B, Wang B, Duan S, Chen Z, Ma W (2017) Novel Dendrimerlike magnetic biosorbent based on modified orange peel waste: adsorption–reduction behavior of arsenic. *ACS Sustain Chem Eng* 5:9692–9700
- Meng X, Korfiatis G, Jing C, Christodoulatos C (2001) Redox transformations of arsenic and Iron in water treatment, sludge during aging and TCLP extraction. *Environ Sci Technol* 35:3476–3481
- Mittal A, Kurup L, Mittal J (2007) Freundlich and Langmuir adsorption isotherms and kinetics for the removal of Tartrazine from aqueous solutions using hen feathers. *J Hazard Mater* 146:243–248
- Nashine A, Tembhurkar A (2016) Equilibrium, kinetic and thermodynamic studies for adsorption of As (III) on coconut (*Cocos nucifera* L.) fiber. *J Environ Chem Eng* 4:3267–3273
- Ofomaja AE, Naidoo EB, Modise SJ (2009) Removal of copper (II) from aqueous solution by pine and base modified pine cone powder as biosorbent. *J Hazard Mater* 168:909–917
- Pena M, Meng X, Korfiatis GP, Jing C (2006) Adsorption mechanism of arsenic on nanocrystalline titanium dioxide. *Environ Sci Technol* 40:1257–1262
- Peter KT, Johns AJ, Myung NV, Cwiertny DM (2017) Functionalized polymer-iron oxide hybrid nanofibers: electrospun filtration devices for metal oxyanion removal. *Water Res* 117:207–217
- Ranjan D, Talat M, Hasan S (2009) Biosorption of arsenic from aqueous solution using agricultural residue ‘rice polish’. *J Hazard Mater* 166:1050–1059
- Renkou X, Yong W, Tiwari D, Houyan W (2009) Effect of ionic strength on adsorption of As (III) and As (V) on variable charge soils. *J Environ Sci* 21:927–932
- Reza RA, Ahmaruzzaman M (2015) A novel synthesis of Fe₂O₃@ activated carbon composite and its exploitation for the elimination of carcinogenic textile dye from an aqueous phase. *RSC Adv* 5:10575–10586
- Sahu UK, Sahu S, Mahapatra SS, Patel RK (2017) Cigarette soot activated carbon modified with Fe₃O₄ nanoparticles as an effective adsorbent for As (III) and As (V): material preparation, characterization and adsorption mechanism study. *J Mol Liq* 243:395–405
- Santra D, Sarkar M (2016) Optimization of process variables and mechanism of arsenic (V) adsorption onto cellulose nanocomposite. *J Mol. Liq* 224:290–302
- Setyono D, Valiyaveetil S (2014) Chemically modified sawdust as renewable adsorbent for arsenic removal from water. *ACS Sustain Chem Eng* 2:2722–2729
- Subramanian K, Kumar PS, Jeyapal P, Venkatesh N (2005) Characterization of ligno-cellulosic seed fibre from *Wrightia tinctoria* plant for textile applications—an exploratory investigation. *Eur Polym J* 41:853–861
- Tian Y, Wu M, Lin X, Huang P, Huang Y (2011) Synthesis of magnetic wheat straw for arsenic adsorption. *J Hazard Mater* 193:10–16
- Van Vinh N, Zafar M, Behera S, Park H-S (2015) Arsenic (III) removal from aqueous solution by raw and zinc-loaded pine cone biochar: equilibrium, kinetics, and thermodynamics studies. *Int J Environ Sci Technol* 12:1283–1294
- Venkatesan G, Narayanan SL (2018) Synthesis of Fe₂O₃-coated and HCl-treated bauxite ore waste for the adsorption of arsenic (III) from aqueous solution: isotherm and kinetic models. *Chem Eng Commun* 205:34–46
- Weber WJ, Morris JC (1963) Kinetics of adsorption on carbon from solution. *J Sanit Eng Div* 89:31–60
- Wilson D, Langell M (2014) XPS analysis of oleylamine/oleic acid capped Fe₃O₄ nanoparticles as a function of temperature. *Appl Surf Sci* 303:6–13
- Wu K, Liu R, Li T, Liu H, Peng J, Qu J (2013) Removal of arsenic (III) from aqueous solution using a low-cost by-product in Fe-removal plants—Fe-based backwashing sludge. *Chem Eng J* 226:393–401

- Yoon Y, Zheng M, Ahn Y-T, Park WK, Yang WS, Kang J-W (2017) Synthesis of magnetite/non-oxidative graphene composites and their application for arsenic removal. *Sep Purif Technol* 178:40–48
- Yoshida I (1981) Adsorption of arsenic (III) ion on various ion exchange resins loaded with iron (III) and zirconium (IV). *Bull Chem Soc Jpn* 3:379–384
- Yu F, Sun S, Ma J, Han S (2015) Enhanced removal performance of arsenate and arsenite by magnetic graphene oxide with high iron oxide loading. *Phys Chem Chem Phys* 17:4388–4397
- Yu X, Tong S, Ge M, Zuo J, Cao C, Song W (2013) One-step synthesis of magnetic composites of cellulose@ iron oxide nanoparticles for arsenic removal. *J Mater Chem A* 1:959–965
- Zhang S, Li X-y, Chen JP (2010) An XPS study for mechanisms of arsenate adsorption onto a magnetite-doped activated carbon fiber. *J Colloid Interface Sci* 343:232–238
- Zhang W, Zheng J, Zheng P, Tsang DC, Qiu R (2015) Sludge-derived biochar for arsenic (III) immobilization: effects of solution chemistry on sorption behavior. *J Environ Qual* 44:1119–1126
- Zhao Z, Jia Y, Xu L, Zhao S (2011) Adsorption and heterogeneous oxidation of As (III) on ferrihydrite. *Water Res* 45:6496–6504
- Zhou S, Wang D, Sun H, Chen J, Wu S, Na P (2014) Synthesis, characterization, and adsorptive properties of magnetic cellulose nanocomposites for arsenic removal. *Water Air Soil Pollut* 225:1945